Nanoscale Wetting Under Electric Field from Molecular Simulations

ARTICLE *in* TOPICS IN CURRENT CHEMISTRY · JULY 2011

Impact Factor: 4.46 · DOI: 10.1007/128_2011_188 · Source: PubMed

3 AUTHORS, INCLUDING:

Christopher David Daub
Norwegian University of Sci…

29 PUBLICATIONS **417** CITATIONS

SEE PROFILE

Top Curr Chem (2012) 307: 155–180
DOI: 10.1007/128_2011_188

Published online: 19 July 2011

Nanoscale Wetting Under Electric Field from Molecular Simulations

Christopher D. Daub, Dusan Bratko, and Alenka Luzar

Abstract Applying an electric field is a well-established experimental method to tune surface wettability. As accessible experimental length scales become shorter, the modification of interfacial properties of water using electric field must come to grips with novel effects existing at the nanoscale. We survey recent progress in understanding these effects on water interfacial tension and on water-mediated interactions using molecular simulations. We highlight the key role of external conditions in determining the system's response to applied electric field. We further discuss the role of appropriate boundary conditions in modeling polar fluids subject to collective polarization. The work reviewed here broadens the basic understanding of applied and internal field effects that can operate in condensed phase systems, from modulating local hydrophilicity/hydrophobicity of engineered and biological surfaces, to surface manipulation in nanofluidic devices.

Keywords Confined water · Interfacial hydrogen bonds · Nanofluidics · Nanoparticle ordering · Nanoscale electrowetting

Contents

C.D. Daub, D. Bratko and A. Luzar (✉)
Department of Chemistry, Virginia Commonwealth University, Richmond, VA 23284-2006, USA
e-mail: dbratko@vcu.edu; aluzar@vcu.edu

1 Introduction

Modulation of solid/liquid interfacial tension by the applied electric field is currently enjoying explosive growth in a wide range of applications: from electrospray ionization and ink-jet printing to electrical control of optical devices [1, 2]. Understanding the influence of an applied electric field on interfacial properties of water is of great interest to workers in the field of microfluidics [3, 4], in particular the electrowetting on dielectric (EWOD) [5]. There is also great interest from the biology perspective since strong fields E (water dipole energy $\boldsymbol{E}\cdot\boldsymbol{d}$ comparable to thermal energy $k_{\mathrm{B}}T$) arise in ion channels of cell membranes [6–10], in membrane electroporation [11, 12], and at the active site on an enzyme [13]. Recent experiments [14–17] investigated the effect of electric field on contact angle, which also potentially impacts the stability of liquid–liquid interfaces [18] and may be pertinent to carbon nanotube sieves of O (1 nm) thickness [19]. There are excellent review articles on electrowetting from macroscopic perspective that the reader is referred to [16, 20–23].

The advent of micro- and nanoporous materials sparked renewed interest in wetting techniques including electrowetting in nanomaterials whose high surface-to-volume ratio makes these media especially difficult to permeate with water. Rapid developments in nanofluidics warrant a transition from continuum to molecular level descriptions [24]. Computer simulation offers unique possibilities for investigating molecular-level phenomena difficult to probe experimentally [25]. In this review chapter we focus on nanoscale effects that can currently be probed best via molecular simulations. These tools give us the predictive power to discover novel effects operating at short length scales.

The chapter is organized as follows. We start with macroscopic thermodynamic predictions and discuss the phase behavior of confined liquids in general in the absence of applied electric field. The primary focus is on capillary evaporation, a phenomenon that can be reversed in the presence of the electric field. The reader is directed to extensive excellent reviews [26] of capillary condensation. Next we focus on the combined effect of confinement and electric field on liquids structure and thermodynamics, water in particular, its stability against evaporation, and resilience of the hydrogen bond network in polarized water. We devote increased attention to issues of external conditions, as they determine how the system responds to applied electric field. We concentrate on systems maintaining

equilibrium with external bath at ambient temperature and pressure. Next we review novel nanoscale effects in electrowetting where polarity and field direction come into play. We briefly describe the method for calculating wetting free energies (and associated contact angles) in a field-exposed nanopore from pressure tensor calculations. We describe a novel mechanism for nanoparticle alignment, based on the notable dependence of surface free energy on the angle between applied field and nanoparticle surface. We end with conclusions and future possibilities.

2 Continuum Thermodynamics

2.1 *Confinement Effects on Liquids*

Spatial confinement can have significant effects on the phase behavior of a confined fluid compared to its bulk counterpart. Classical examples are the shift of the bulk gas–liquid condensation in adsorbing confinement towards lower pressures (capillary condensation), or shift towards higher pressures [27] in a lyophobic confinement (capillary evaporation) [28] and the corresponding shift of the vapor–liquid critical point [29–31]. In a simulation study of strongly coupled dipolar fluids (spherical particles with permanent point dipoles), Klapp and Schoen showed that the presence of confining walls can promote long-range parallel ordering of the dipoles [32, 33].

Confining a liquid between weakly attractive lyophobic surfaces (characterized by contact angles above 90°) at a sufficiently small separation will lead to spontaneous evaporation. This thermodynamic process is controlled by competition between bulk energetics (that favors the liquid phase) and surface energetics (that favors the vapor phase). The liquid-to-vapor transition occurs when the grand potential of the confined liquid and confined vapor are comparable [28, 34, 35]:

$$\Omega_{\mathrm{l}} \sim -PV + 2A_{\mathrm{w}}\gamma_{\mathrm{wl}} = \Omega_{\mathrm{v}} \sim -P_{\mathrm{v}}V + 2A_{\mathrm{w}}\gamma_{\mathrm{wv}} + A\gamma \tag{1}$$

where $V = A_{\mathrm{w}}D$ is the volume of the confined region, $A_{\mathrm{w}} \propto L^2$ the wetted area of the wall, and $A \propto LD$ the area of the liquid/vapor interface. The A term is relevant because of finite lateral size. For an incompressible fluid the difference in the bulk pressure, P, and the pressure of the coexisting vapor, P_{v}, can also be replaced by $\rho\Delta\mu$ [36, 37], where ρ is the number density of the liquid and $\Delta\mu$ is the difference in the chemical potential of bulk liquid from the value at liquid–gas coexistence.

From the above equality, the general expression for the critical threshold distance for spontaneous expulsion of a liquid confined between surfaces of the *finite* lateral size, L, follows [28]:

$$D_{\mathrm{c}} = 2\Delta\gamma/(P - P_{\mathrm{v}} + b\gamma/L), \tag{2}$$

where

$$\Delta\gamma = \gamma_{\mathrm{wl}} - \gamma_{\mathrm{wv}} = -\gamma\cos\theta_{\mathrm{c}} \tag{3}$$

is the Young equation [38] relating the difference in wall/vapor and wall/liquid surface tension to the surface tension of the free liquid–vapor interface, γ, and the contact angle θ_{c}. b is a geometry dependent constant of the order of unity. Equation (2) shows that for (laterally) small confinements, the critical separation approaches the confinement lateral size, $D_{\mathrm{c}} = O(L)$. Berne and coworkers have used an analogous equation (2) to study capillary-evaporation induced collapse of ellipsoidal hydrophobic particles [34, 39]. For macroscopic surfaces $L \to \infty$, and $P \gg P_{\mathrm{v}}$, (2) reduces to the well-known Kelvin equation [40],

$$D_{\mathrm{c}} \simeq 2\Delta\gamma/P. \tag{4}$$

The thermodynamic effects of finite size and the kinetic barriers, ΔG^*, for the formation of vapor phase have been fully developed [41–46]. Macroscopic thermodynamics predicts that when we have two non-polar surfaces immersed in a liquid and bring them closer together, at a critical distance, D_{c}, liquid will be replaced by vapor (2). Due to a considerable free energy barrier for confinement-induced evaporation, however, the liquid phase is often metastable below D_{c} [36, 41, 43, 45, 47]. Coarse-grained simulations confirmed [45] macroscopic scaling predictions [48, 49]:

$$\Delta G^* \propto D^2, \quad \Delta G^* \propto 1/\cos\theta_{\mathrm{c}}. \tag{5}$$

Combining the known result for the magnitude of the activation barrier and the evaporation rate of molecular water in a specified molecular confinement [41] with the above scaling results enables predictions of kinetic viability of expulsion of water over a range of length scales and between arbitrary physically and chemically modified hydrophobic surfaces with contact angles above 90°. In many practical situations the activation barrier for evaporation can lead to a strong metastability of confined liquid phase. For extended, strongly hydrophobic nanopores ($\theta_{\mathrm{c}} \sim 135^\circ$), widths above ~1.6 nm proved sufficient to suppress capillary evaporation kinetically over practical simulation times [36, 41].

Extrapolation from intermediate to lower contact angles (closer to 90°) enables estimating ΔG^* at conditions where critical cavity sizes and barrier magnitudes make simulations impractical even for coarse-grained models [45]. This regime is important because low contact angles slightly above 90° are characteristic of many so-called hydrophobic surfaces observed in nature. If the relation $\Delta G^* \sim 1/\cos\theta_{\mathrm{c}}$ is approximately valid, reducing the contact angle from, say 110–100° nearly doubles the barrier to evaporation. In view of barrier values for $\theta_{\mathrm{c}} = 109^\circ$ (Fig. 6 in [45]), it is clear that in most naturally occurring systems we cannot expect to observe spontaneous evaporation except from a small molecular-sized confinement.

These predictions [45] have been confirmed in studying the capillary evaporation events within hydrophobic pockets of melittin dimers [50].

When the liquid-to-vapor transition is suppressed kinetically, the loosening of water structure characteristic of hydrophobic interfaces (so-called soft interfaces [51, 52]) can still be inferred from the rise in compressibility, κ, within the solvation layer. The increase in surface compressibility of water has been quantified from density fluctuations [36] and direct density dependence on the pressure [43]. Compressibility next to hydrophilic surfaces, on the other hand, remains virtually indistinguishable from that of bulk water [43, 53]. Local compressibility has also been shown to offer a viable measure of hydrophobicity at a molecular level [52, 54]. The issue will be addressed in the following sections as we describe the changes in surface compressibility revealed in a simulated electrowetting experiment.

2.2 *Combined Effects of Confinement and Electric Field: Electrocapillarity*

If an electric field is applied across the planar confinement, additional contributions reducing the wetting surface free energy (3) arise. Electrocapillarity can reverse the sign of $\cos\theta_c$, leading to *electrowetting* of a lyophobic surface. Ignoring any field dependence of liquid/vapor (γ) and solid/liquid (γ_{sl}) surface tensions, within continuum approximations, the macroscopic relation due to Lippmann [55] describes electrocapillarity by

$$\cos\theta_c(V) = \frac{\gamma_{sl} - \gamma_{sv}}{\gamma} - \frac{W_{el}(V)}{\gamma} = \cos\theta_o - \frac{W_{el}(V)}{\gamma}. \tag{6}$$

Here $W_{el}(V)$ is the change in electrostatic energy per unit area, associated with surface spreading of the liquid wetting both walls, V is the voltage across the interface, and θ_o is the contact angle in the absence of electric field. Precise form of W_{el} depends on system geometry and material properties but is generally presumed to be proportional to the areal electric capacitance of the interface, c, and the potential drop across the interface squared, $W_{el} \sim -cV^2/2$ [16, 20]. Inserting Lippmann's effective surface tension into Young's equation (3), we obtain the electrowetting Young-Lippmann equation:

$$\cos\theta_c = \cos\theta_o + cV^2/2\gamma \tag{7}$$

which describes the low voltage behavior of the contact angle [20, 56].

In macroscopic experiments, electrocapillarity effects usually originate in a thin surface layer where electric field is strong [20, 38]. In microscopic pores, on the other hand, the field permeates throughout the whole aqueous slab. Notwithstanding its

weak ionization, pure water in a nanopore can be considered to behave as a dielectric of relative permittivity ε because the double layer screening length associated with water ions exceeds the nanopore width by orders of magnitude. The field E_o can stem from charges on the plates of a capacitor [15] or can be attributed to charges in the nearby environment. Water can enter the confinement from external field-free reservoir at ambient temperature and pressure, hence the state of confined water is fully described by specifying the values of chemical potential μ, volume A_wD ($A_w \gg D^2$ is the plate area and D inter-plate separation), temperature T, and field strength E.

For a uniform field, the continuum level approximation for the difference between electrical energies of water-filled (l) and empty (e) pores, treated as capacitors with areal capacitances $c_e = \varepsilon_0/D$ and $c_l = \varepsilon_r\varepsilon_0/D$, gives [7]

$$W_{el} = W_l - W_e \cong \frac{D}{2}(\varepsilon_r\varepsilon_0 E^2 - \varepsilon_0 E_0^2) \approx -\frac{\varepsilon_0 D}{2}E_0^2. \tag{8}$$

In (8), $E_0 = V_0/D$ is the applied electric field across the slit before reduction due to water polarization ($E_o \to E = O(E_o/\varepsilon_r)$). Equations (6) and (7) suggest an expression for apparent contact angle $\cos\theta_c \sim \cos\theta_c{}^o + \varepsilon_o D{E_o}^2/4\gamma$. Here, W_{el} is associated with volume rather than with the surface layer alone. Equation (6) also presumes that bare surface tensions, γ_{ab} (a, b = s, l, v) remain unaffected by the field. While the latter is usually true for the solid–vapor term, γ_{sv}, the alignment of water molecules in the field can modify molecular interactions at the surface and hence further affect γ_{sl} *and* γ_{lv}, an effect confirmed by simulations (see Sect. 4.2).

Favorable interaction of a polar liquid with electric field also results in increased liquid density ρ. To the first order, electrostriction is given by

$$d\ln\rho = \frac{\kappa\rho}{8\pi}\frac{\partial\varepsilon}{\partial\rho}d(E^2), \tag{9}$$

where E is local field and κ is isothermal compressibility [57, 58]. In common with predictions for other geometries [16], in weak fields (7) and (8) imply that the change in contact angle and relative increase in local density vary in proportion to field squared. Equations (6) and (7), combined with an appropriate estimate of areal capacitance of the surface, provide the basis for techniques to tune hydrophobic/hydrophilic surfaces electrically [20, 59, 60] while (8) offers a qualitative explanation of the role of ions in gating of biological channels [6, 7, 61].

As already discussed, in narrow hydrophobic confinements, unfavorable surface energetics can trigger capillary evaporation if $D < D_c$ [(2) and (4)] [36, 41, 44, 46, 48, 49], provided the kinetic barriers are surmountable [45]. Dzubiella and Hansen discussed a generalization of Kelvin equation that incorporates the effect of electric field [62]. The energy density change due to the field augments the PV term, which tends to suppress liquid expulsion, thus reducing the threshold separation D_c. For an extended planar confinement subject to a weak electric field E_o, the generalized relation takes the form [63]

$$D < -2\gamma_{\mathrm{lv}}\cos\theta_0 / \left(P + \frac{\varepsilon_0 E_0^2}{4\gamma_{\mathrm{lv}}}\right). \tag{10}$$

The extended expression enables studies of phase instability in dispersions of charged particles like ionic colloids. In the context of this review, it helps to explain electrostriction or electrowetting in a confinement maintaining equilibrium with a field-free aqueous bath. Brunet et al. discussed the use of electric field to tune mixing/demixing equilibria in a multicomponent system [64, 65].

3 Molecular Thermodynamics

3.1 Water in Hydrophobic Confinement and Applied Field

Stabilization of liquid phase under an applied field conforms to experimental observations of electrostriction as the field attracts more water into the exposed region. The behavior is captured in several simulation studies, both in the bulk [66, 67] and confined [7, 53, 61, 66, 68] regimes. On the other hand, some studies reported field induced depletion or evaporation in bulk [69] and confined [57] water; hence it is of interest to discuss the underlying differences between these works.

Some of these differences can be attributed to different thermodynamic conditions (Fig. 1). Studying confined water in a field-exposed confinement, open to water flow from the external, field-free bath, is an entirely different situation from the case of an isobaric system, closed to water exchange. In the former scenario, water in confinement responds to applied field by increasing the density

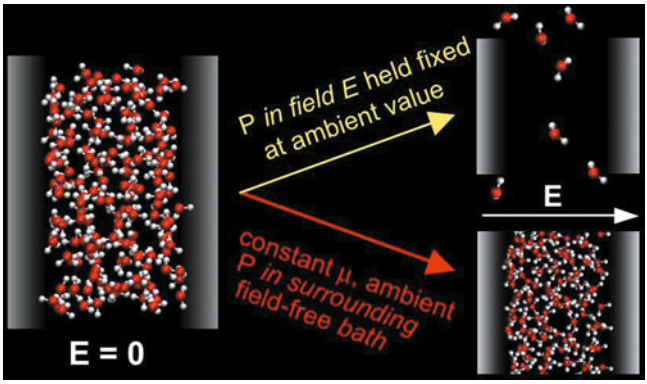

Fig. 1 Imposed external conditions lead to different responses of confined water to electric field. *Left*: field free water in a hydrophobic confinement. *Right*: field-exposed systems. *Top*: isobaric, mass conserving system of variable lateral dimensions. *Bottom*: isochoric confinement subject to applied field, and open to exchange of water with field-free aqueous bath

to equalize its chemical potential with that in the external bath. In the closed isobaric system, the amount of water is fixed and volume adjusts to maintain pressure constant despite the application of the field.

The response of the volume V in a mass-conserving isobaric (N, P, T) system to the application of field E_o=|$\boldsymbol{E_o}$| can be described by

$$\frac{\partial < V >}{\partial E_o} = \frac{\partial}{\partial E_o}\left(\Delta^{-1}\sum_{V_j}\sum_{\text{states } i} V_j e^{-\frac{U_i}{k_B T}-\frac{pV_j}{k_B T}}\right)$$
$$= -(k_B T)^{-1}\left(< V\frac{\partial U}{\partial E_o} > - < V >< \frac{\partial U}{\partial E_o} >\right) \quad (11)$$

where $\Delta = \sum_{V_j}\sum_{i} e^{-\frac{U_i}{k_B T}-\frac{pV_j}{k_B T}}$.

Each of states i corresponds to a distinct configuration [$\boldsymbol{r}_N$, $\boldsymbol{\Omega}_N$] consisting of positions $\boldsymbol{r}$ and orientations $\boldsymbol{\Omega}$ of all N particles. The angle brackets denote the ensemble average. The slope $\partial U/\partial E_o$ measures the ease with which the molecules align with the field, and can increase with fluid dilution. All N molecules are exposed to the field and any structural rearrangement takes place only to find the best compromise between molecular alignment with the field and orientation-dependent interactions among molecules. The density of a mass-conserving isobaric polar fluid can therefore decrease under applied field E_o. The prediction agrees with the (N, P, T) simulation in [69] but is not transferable to other external conditions.

Electrowetting experiments typically involve transfer of water from a field-free region or region with weak field to a region under strong field to maximize field/dipole interaction [20]. Pressure is therefore neither fixed nor uniform, but the chemical potential of an equilibrated system is uniform. These thermodynamic conditions are best described by grand canonical (μ, V, T) statistics with fixed volume (V), temperature, and chemical potential μ. The field dependence of the mean number of molecules, $<N>$, in the field-exposed region is given by

$$\frac{\partial < N >}{\partial E_o} = \frac{\partial}{\partial E_o}\left[\Xi^{-1}\sum_{N}\sum_{\text{states } i} N e^{-\frac{U_i}{k_B T^{-1}}+\frac{\mu N}{k_B T^{-1}}}\right]$$
$$= -\frac{1}{k_B \mathrm{T}}\left(< N\frac{\partial U}{\partial E_o} > - < N >< \frac{\partial U}{\partial E_o} >\right) \quad (12)$$

with $\Xi = \sum_{N}\sum_{i} e^{-\frac{U_i}{k_B T}+\frac{\mu N}{k_B T}}$.

Electric field $\boldsymbol{E_o}$ affects the energy U through orientation-dependent interaction with molecular dipoles d, $U(N) = -E_o\sum_1^N d_i\cos\theta_i = -NE_o d\overline{\cos\theta}$:

$$\begin{aligned}\partial N/\partial E_o &= \frac{d}{k_B T}\left(< N^2 \frac{\partial(E_o \overline{\cos\theta_{N,i}})}{\partial E_o} > - < N >< N \frac{\partial(E_o \overline{\cos\theta_{N,i}})}{\partial E_o} >\right) \\ &= \frac{d}{k_B T}\left(< N^2 \overline{\cos\theta_{N,i}} > - < N >< N \overline{\cos\theta_{N,i}} >\right),\end{aligned} \tag{13}$$

where $d=|\boldsymbol{d}|$. $\overline{\cos\theta_{N,i}}$ measures the average dipole alignment, $\boldsymbol{d}\cdot\boldsymbol{E_o}/|\boldsymbol{d}||\boldsymbol{E_o}|$, of N molecules in the system in configuration (N,i), because $\overline{\cos\theta_{N,i}} \geq 0$ for all representative configurations, and the *product* $(N\overline{\cos\theta_{N,i}})$ generally increases with N. The density of a dipolar liquid in an open system will therefore rise with increasing field strength E_o as predicted by continuum analyses [57, 70, 71] and seen in electrostriction experiments.

Simulation studies for bulk and confined systems at different external conditions have been compared over a range of applied electric fields. Open (μ, V, T) systems invariably show density increase under applied field, both in bulk and confined phases, with or without Ewald periodic conditions. Bigger effects are restricted to hydrophobic confinements, as water fills the initially depleted interfacial layers. On the other hand, dilution and eventual evaporation are observed in mass conserving, isobaric systems when constancy of pressure is enforced in the presence of the field. Representative results are collected in Fig. 2.

3.1.1 Electric Fields in Modeled Systems

A few comments pertaining to simulation studies of field-exposed aqueous systems discussed in this review are in order to aid in evaluating the results, presented in Fig. 2 and in subsequent sections.

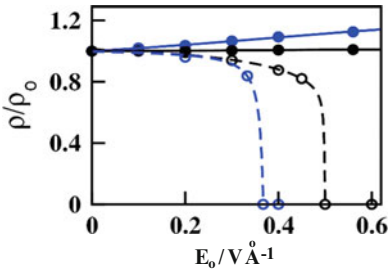

Fig. 2 Simulated water density dependence on the strength of (unscreened) applied field $0 \leq E_o \leq 0.6$ V Å^{-1}. The actual field, E, is lowered by orientational polarization of water, and spans the range $0 \leq E \leq 0.025$ V Å^{-1}. In confinement, dielectric screening renders the field both weaker *and* nonuniform. *Blue*: 1.64 nm wide hydrophobic confinement (wall contact angle 135°), *black*: bulk water. *Solid lines* and *circles* describe open systems (varying N) under the field, in equilibrium with field-free water bath. *Dashed lines* and *open symbols*: closed (mass conserving) isobaric systems. To keep pressure constant, these systems expand under the field. Note that different conditions (μ,V,T) (*solid symbols*) vs (N,P,T) (*open symbols*) correspond to *contrasting physical situations*, and *not* the same situation described using different ensembles

First, the reported field strengths warrant explanation. In the absence of tin-foil boundary conditions [72, 73], the actual strength of electric field spanning the aqueous phase, $\boldsymbol{E}(r)$, differs significantly from the unperturbed "applied" field $\boldsymbol{E_o}$ due to the opposing effect of water polarization. The actual, dielectrically screened field $\boldsymbol{E}(\boldsymbol{r})$ is generally nonuniform and is of the order ε_r^{-1} weaker than the unscreened field $\boldsymbol{E}_o$. In the bulk phase, modeled by Ewald summation with vacuum boundary conditions [72], the exact relation (for the absolute values of the field) is $E = 3E_o/(\varepsilon_r + 2)$, where ε_r is the relative permittivity [74]. While constant-voltage simulation techniques have been presented [75, 76], in most cases, E_o represents input information for a simulation experiment and the screened, position dependent, field $\boldsymbol{E}(r)$ can be determined during the simulation. In the latter case, a viable estimate of the average field $\overline{E}$ across the system can be obtained from the observed polarization of water, measured in terms of the cosine of the alignment angle, $\overline{< \cos\theta_{N,i} >}$ [77–79]. When compared with a laboratory measurement, a simulation with fixed applied field E_o is akin to an experiment on a system between electrified surfaces (or capacitor plates) with fixed charge densities. The common fixed-voltage experiment, on the other hand, corresponds to preselecting the average field across the system. The implications of the two different constraints have been discussed by Jia and Hentschke [80]. In capturing electrostatic screening in a globally polarized system, simulations employing Ewald periodic conditions are generally superior to cutoff-based techniques. While the use of a distance cutoff on the intermolecular interactions mostly gives a satisfactory qualitative description of the system's responses to the field, dielectric screening is typically underestimated, and the average field $\overline{E}$, and apparent voltage V across the system, $V \sim D\overline{E}$ are overestimated in this approach [68]. For clarity, both the exact value of the unscreened input field E_o and the approximate average of the actual field will be listed in most cases we discuss below.

The second comment concerns the usage of rigid water models such as the SPC/E model [81], which by design cannot undergo ionization or react chemically. We note that actual fields considered here are much too weak to polarize significantly, let alone decompose water when any flow of electric current is prevented by proper insulation. Top end insulators like polymer and silica films with dielectric strength of up to 5×10^8 V m^{-1} can provide more than adequate insulation.

3.2 Resilience of the Hydrogen Bond Network in Polarized Water

For an open system, described by (13), any field-induced density depletion, $(\partial N/\partial E_o)_{\mu VT} < 0$, could only be expected in case of dramatic rise in orientational polarizability of the molecules upon dilution. A mean-field analysis [69, 82] of a water-mimicking Ising model in electric field explored the assumption that molecular dipole alignment perturbs hydrogen bonding. Over an interval of intermediate field strengths, the model-system featured a density drop akin to the

reported evaporation from an open, field-exposed confinement [57] in equilibrium with unperturbed bath. Repeated observations of electrostriction (density increase under field) in other simulation studies of open systems [6, 7, 61, 63, 66–68] question the hypothesis [69] of strongly negative correlation between attractive water–water interactions (dominated by hydrogen bonding), and water's ability to align with the applied field.

The issue was addressed in Monte Carlo and Molecular Dynamics simulations directly monitoring water structure and the extent of hydrogen bonding as the molecules became increasingly aligned by the applied field [68]. Below, we report results for fields E_o up to 0.8 V Å^{-1}, corresponding to actual fields of up to 0.03 V Å^{-1}, thus spanning the range of fields detectable near charged electrodes, ion channels, ionic biomolecules or assemblies [6, 79, 83–93]. Within the above range of fields, no significant field-induced changes in water hydrogen bond populations, in atom–atom distribution functions or in water's tetrahedral coordination were observed [68]. The resilience of hydrogen-bond strength and their population were confirmed by:

1. Direct population statistics: the number of bonds does not diminish upon polarization by the field.
2. The average energy of the bonds remained essentially equal to that in field-free water.
3. The preserved *free-energy* advantage of forming bonds was evidenced by unperturbed equilibrium between the populations of formed and ruptured bonds. Any weakening in the *free-energy* of the bonds in the field-oriented water would be reflected in at least some increase in the fraction of ruptured bonds, which did *not* happen.

Simulation results demonstrate that high alignment of aqueous dipoles can be achieved without serious penalties in the number and free-energies of hydrogen bonds or distortion of tetrahedral coordination. An onset of the transition from tetrahedral toward tightly-packed, highly coordinated "electrofrozen" structure can be observed at extreme fields of about 2 V Å^{-1} and higher [79, 94, 95]. Remarkable persistence of the hydrogen-bond network under aligning electric field equal or below 1 V Å^{-1} is evidenced by several studies [79, 88, 96–98] showing no evidence that field alignment would be conducive to unraveling of the hydrogen bonded network. For uniform phases, recent Gibbs ensemble simulations by Sieppman and coworkers [67] explicitly confirm that orientational polarizability of water molecules in liquid phase exceeds that in vapor.

A common Molecular Dynamics approach in studies of confined systems at fixed chemical potential employs an isobaric, bulk-like bath surrounding the confinement. The conditions inside a field-exposed confinement (e.g., inside a capacitor) should therefore be close to (μ, V, T) ones of GCMC cases [66, 68], suggesting similar electrostriction behavior. Occurrence of a field-induced expulsion of water has, however, been reported in a Molecular Dynamics study of this kind [57]. To secure proper barostat performance under strongly nonuniform and anisotropic pressure fields, and to account for the discontinuity between field/no

field regimes (impulse on crossing molecules) in (*N, P, T*) Molecular Dynamics are still open technical challenges. Avoiding explicit boundaries between field and no-field regions, Grand Canonical [61, 66, 68] and Gibbs ensemble [67] Monte Carlo approaches represent natural choices for molecular studies of electrowetting under nonuniform applied field. Local Molecular Field (LMF) theory [99] is poised to offer a promising alternative to molecular simulations in electrically nonuniform systems.

4 New Effects at the Nanoscale

Traditionally, electrowetting has been considered a relatively non-specific phenomenon defined in terms of a material's macroscopic properties. The effect of applied field on $\cos\theta_c$ has generally been found to be proportional to voltage squared, independent of field polarity and direction, as in (7). Nanosized aqueous confinements we review next, however, behave very differently from macroscopic systems. Due to molecular anisotropy of water, the electric field effect on the surface tension at aqueous interfaces *depends on the angle* between the field and the surface. The field-induced alignment competes with orientational preferences of interfacial water molecules relative to a wall to maximize hydrogen bonding [100–103]. The two trends are reconciled when the field is parallel to the interface. Perpendicular field, on the other hand, results in asymmetric wettability of opposing confinement surfaces (Fig. 3). These nanoscale effects, in contrast to conventional macroscopic experiments, derive primarily from the properties of the first solvation layer, and are negligible in systems of macroscopic dimensions. Analogous direction dependence is observed in sessile nanodroplets' response to electric field [104]. Preferred alignment of confinement surfaces with the field suggests a novel mechanism whereby the applied electric field can orient nanoparticles even in the absence of charges or dielectric contrast.

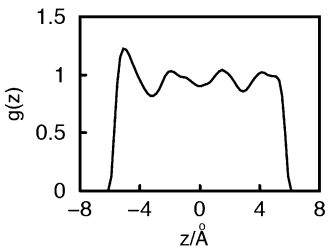

Fig. 3 Simulated density profile of water in an extended hydrophobic (hydrocarbon-like) nanopore subject to normal electric field of strength 0.2 V Å^{-1} (average actual field $E \sim 0.005$ V Å^{-1}) in equilibrium with a field-free aqueous reservoir. Model: SPC/E water. Method: GCMC with slab-corrected Ewald sums for laterally periodic boundary conditions

Examples discussed below illustrate field-direction effects in selected scenarios. Avoiding possible ambiguities related to the angle between the surface and the applied field in the presence of surface roughness, these examples focus on smooth interfaces described by two forms of substrate/water interaction. The integrated, laterally invariant Lennard-Jones (9–3) potential [102] was used in nanopores as it allows lateral scaling, thus facilitating surface free energy calculations [53, 66]. The Grand Canonical Transition Matrix Monte Carlo approach developed by Errington and coworkers enables extensions to nonplanar surfaces [105, 106]. Interfacial behavior at smooth surfaces was consistent with that observed on molecular substrates mimicking graphitic surfaces in sessile drop [104], thin films [107], and suspended nanoparticle calculations [108].

4.1 Effects of Field Direction and Polarity on the Wetting Properties

Molecular simulations of water equilibrium between nanopores under electric field and unperturbed bulk phase demonstrated notable differences between electrowetting at the nanoscale and in macroscopic systems [53, 66, 68]. Due to the coupling between surface/water and field/water forces, the water/wall surface tension depends on the alignment between the surface and the field. This, in turn, reflects in angle-dependent uptake of water in the pore. The transition from hydrophobic to hydrophilic behavior of paraffin-like nanopores upon imposition of electric field is enhanced when the field is parallel with confinement walls. In a narrow, 1.64 nm wide planar pore (a width just above kinetic threshold to capillary evaporation from a hydrocarbon-like pore [41]), simulated by GCMC, electrostriction (solid blue curve in Fig. 2), is about twice the strength in parallel vs normal fields. In a normal field, the coupling of field-induced alignment and orientational preferences of interfacial water molecules *relative to a wall* renders solvation layers at opposing walls completely different. As shown in Fig. 3, the hydrophobic wall under incoming field (pointing into aqueous phase) features a pronounced density peak of water/wall distribution function, $g(z)$, in the first solvation layer, reminiscent of hydrophilic hydration. The opposite wall, on the other hand, shows essentially no peak, in analogy with hydrophobic solvation in the absence of the field [66, 68]. Polarity dependence of water density profiles have also been reported between oppositely charged colloids [63] and between parallel graphene sheets under strong electric field [57]. When the field is applied along the walls, prominent hydration peaks form at both walls [66]. The sensitivity to field direction and polarity is explained by competition between spontaneous water molecule-surface orientations and molecular dipole alignment with the field. As do all polar fluids, aqueous dipoles prefer polarization parallel to walls. This general tendency acts in concert with orientational ordering imposed by hydrogen bonding. Under the *combined* effects, the optimal orientation of interfacial water molecules corresponds to dipoles almost aligned with the wall, but pointing slightly into the

liquid phase. Electrowetting is therefore most effective when the field polarizes water along the wall, but is considerably weaker when the field tends to turn water dipoles *toward* the wall. Consistent with the above picture, hydrogen bond populations, monitored as a function of field angle relative to the walls, are enhanced in parallel fields and depleted especially at interfaces with field pointing toward the wall [66]. Analogous preference for the interface/field alignment has been observed and discussed in recent simulation studies of nanodroplet elongation [109] and aqueous film evaporation [110] in the field. The surprisingly strong effect of field direction and polarity on surface wetting is a signature of the nanoscale regime where surface molecules represent a statistically significant constituency.

4.2 Wetting Free Energy

Field-enhanced wettability can be quantified in terms of wetting surface free energy, $\sigma(E)$, here defined as the sum $\Delta\gamma + W_{el}(E) = -\gamma\cos\theta_c(E)$ [(3) and (6)]. For smooth surfaces, σ inside an open nanopore of fixed width D has been shown [66] to relate to the lateral component of the pressure tensor, $P_{\|}$:

$$\sigma = \frac{\partial\Omega}{\partial A} = -\frac{P_{\|}D}{2}. \tag{14}$$

Here, Ω is the grand potential of the wetted part of the confinement atop the wetted area A with volume AD. A recent study reported systematic GCMC calculations of $\sigma(E)$ in hydrocarbon-like nanopores [66]. To estimate contact angles under the field also required calculations of surface tension (γ_{lv}) as a function of the field strength. Calculations for a free-standing aqueous slab were performed using the conventional relation $\sigma(E) = (P_{\perp} - P_{\|})D/2$. A novel finite-difference technique for the calculation of pressure tensor components determined energy differences ΔU_{α}, associated with uniform scaling of molecular coordinates α ($\alpha = z$ or x, y) and volume change ΔV_{α} [66]. $\Delta U_{\alpha} = U_{\alpha}(V + \Delta V_{\alpha}/2) - U_{\alpha}(V - \Delta V_{\alpha}/2)$ comprised changes in intermolecular and water–wall interactions. As described in Supporting Information to [66], pressure tensor components were obtained from the relation

$$P_{\alpha\alpha} = \rho kT + \lim_{\Delta V_{\alpha}\to 0}\frac{kT\ln < \exp(-\frac{\Delta U_{\alpha}}{kT}) >}{\Delta V_{\alpha}} = \rho kT - \lim_{\Delta V_{\alpha}\to 0} < \frac{\Delta U_{\alpha}}{\Delta V_{\alpha}} >. \tag{15}$$

Related finite-difference techniques have been studied in a number of contexts involving fluids with hard-core [111] and soft potentials [112–116]. The central finite-difference approximation, analyzed systematically in [115], was implemented [66] through scaling by a factor of $f = 1 \pm \varepsilon$ with $\varepsilon = 10^{-5}$ in forward and backward directions. Within the range $10^{-6} \le \varepsilon \le 10^{-4}$, no significant dependence on ε has been detected and exponential and linearized forms of (15) produced identical

results. The calculated normal component of the pressure tensor, $P_{zz} \equiv P_{\perp}$, matched the wall pressure calculated directly from wall/water forces as described elsewhere [36]. Consistency of the pressure tensor approach was also verified by direct surface free energy calculations using thermodynamic integration [117]. An interesting variant of thermodynamic integration with phantom wall approach was introduced by Muller-Plathe and coworkers [118]. Pressure, compressibility, and wetting free energies followed the trend described in discussing electrostriction and water structure in the presence of the field. As water is driven into the pore, the pressure rises approximately in proportion to field squared; however, the rise is steeper in a parallel field [66]. The change is accompanied with decreasing interfacial compressibility, approaching that of bulk water in the strong field limit (Fig. 4). Compressibility next to hydrophilic surfaces, on the other hand, proves essentially insensitive to applied field. The nonlinear dependence of compressibility on surface contact angle, highly sensitive at high θ_c and almost insensitive at $\theta_c < 90^\circ$, is illustrated in Fig. 5 [119]. The observed asymmetric dependence conforms to

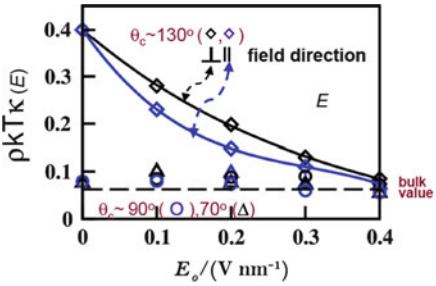

Fig. 4 Reduced compressibility, $\rho k_B T\kappa$, in a planar nanopore of width $D = 1.64$ nm as a function of applied (nonscreened) electric field E_o from Grand Canonical Monte Carlo simulations in SPC/E water for three wall/water contact angles $\theta_c = 135^\circ$ (*diamonds*), 93° (*circles*), or 69° (*triangles*). Actual field E ranging from 0 to 0.0095 V Å^{-1} Reduction in compressibility inside a hydrophobic pore, $\theta_c = 135^\circ$, is indicative of electrostriction in the field. Electrostriction is stronger in parallel than normal field

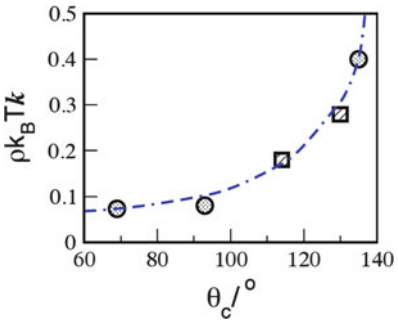

Fig. 5 Reduced compressibility, $\rho k_B T\kappa$, of water in a planar nanopore of width $D = 1.64$ nm as a function of surface contact angle, θ_c in SPC/E water [53, 66, 119]. Contact angle of chemically homogeneous pore walls was varied through surface chemistry (*circles* at $\theta_c = 135^\circ$, 93°, or 69°), or by applying electric field across a hydrophobic pore (*squares* at 114° and 129°)

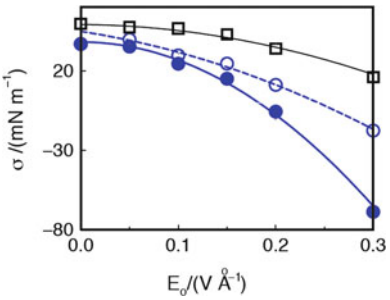

Fig. 6 Wetting free energy $\sigma(E_o)$ in 1.64 nm wide hydrophobic pore as a function of applied field E_o (actual normal field E up to 0.008 V Å^{-1}). *Empty circles*: perpendicular field, *solid symbols*: parallel field, and *squares*: water/air surface tension of a free-standing aqueous slab of identical thickness. Field direction was not significant in the latter case

reported sensitivity to minority polar groups on hydrophobic surface and marginal influence of hydrophobic groups in a polar context [52, 117, 120, 121].

Calculated wetting free energies, shown in Fig. 6, reveal the prominent effect of field direction. In a 1.64 nm wide pore and strong field $E_o \sim 0.3$ V Å^{-1}, the wetting surface free energy in parallel field is nearly 50 mN m^{-1} lower than the average over both walls in a normal field. Again, the fields E_o in Fig. 6 correspond to external field before reduction due to dielectric screening, which renders the field across the pore nonuniform and over an order of magnitude weaker ($\overline{E}$ up to 0.008 V Å^{-1}). Based on the structures of hydration layers (Fig. 3), the solvation of the confinement wall with outgoing normal field is similar to that observed at both walls in the parallel field. The wall with incoming normal field, on the other hand, remains only weakly affected by the field. In sufficiently strong normal field, this asymmetry renders one wall strongly hydrophilic, the other hydrophobic. This situation, known as a Janus interface, shows very interesting behavior experimentally [122]. Janus interface can be produced, for example, by applying voltage of ~0.1 V ($E_0 \sim 0.2$ V Å^{-1}, average field $E \sim 0.005$ V Å^{-1}) across a 2 nm wide confinement, without modifying the surfaces themselves.

4.3 Water-Mediated Ordering of a Nanomaterial

A crucial step in the manufacture of many complex materials is the orientation of the constituents in a solvent such that they can be deposited on a substrate with a desired orderly structure. Several methods have been considered for an efficient solute orientation in a solvent [123, 124], but they all rely on the presence of a nanoparticle permanent dipole or considerable dielectric contrast between the particle and the medium [125, 126]. A newly proposed method of orienting nanoparticles [53] exploits the coupling between the field-alignment of polar solvent molecules and anisotropic solvent–solute interactions due to solvent

molecules' electrostatic and geometrical asymmetry. This coupling can lead to directional solvent–solute forces [66] and torques, which favor certain solute orientations, irrespective of the electric nature of the solute itself. A major contribution to the torque comes from the preference of water to maximize its hydrogen bonding [66, 104], augmenting the general tendency of dipolar fluids to spontaneously polarize parallel to the interface [32, 33, 127, 128]. According to macroscopic electrostatics, electric field will generally align anisotropic particles with dielectric constant *different* from that of the medium. The free energy F of an object of volume V_2 and permittivity ε_2 in the medium ε_1, and associated aligning torque $\tau(\phi)$, is [125]

$$F = \frac{1}{2}\int_{V_2} (\varepsilon_2 - \varepsilon_1)\,\vec{\mathrm{E}}_1 \cdot \vec{E}_2(\vec{r})d^3\vec{r}, |\tau| \sim \left|\frac{\partial F}{\partial \phi}\right| \tag{16}$$

where E_1 is the field in the absence of the particle, E_2 the perturbed field, and ϕ the angle of rotation. At the molecular and nanometer scale, however, significant additional orientational forces operate *without* requiring the nanoparticle to have a dipole moment, or strongly contrasting permittivity. For example, this effect could orient a solute of permittivity close to that of the solvent in a large local electric field next to a DNA polyion (actual field $E = \mathrm{O}(10^{-2})\mathrm{V\ \AA}^{-1}$, $E_\mathrm{o} = \mathrm{O}(1)\mathrm{V\ \AA}^{-1}$) [83].

4.3.1 Nanopore Geometry

Because of the coupling between orientational forces on surface water molecules and their aligning with the field, the wetting free energy of nanopore walls depends on the angle ϕ between the walls and the direction of the field. In a planar pore, the wetting free energy, $\sigma(E, \phi)$, is lowest in the parallel orientation, gradually increasing as the angle ϕ approaches 90°. Figure 7 illustrates this dependence for planar nanopores of two widths, 1.64 and 2.7 nm. The applied field across the pore before accounting for dielectric screening equaled 0.2 V $\mathrm{\AA}^{-1}$, with the average actual field

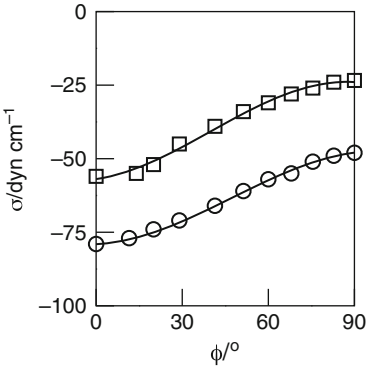

Fig. 7 Wetting free energies inside planar confinements of widths 1.64 (*upper*) and 2.7 nm (*lower curve*) as functions of the angle between the field and the walls. Field strength: $E_\mathrm{o} = 0.2$ V $\mathrm{\AA}^{-1}$, average actual field $E \sim 0.005$ V $\mathrm{\AA}^{-1}$ (at $\phi = 90^\circ$), wall contact angle 93°

of O(10^{-2}) V Å^{-1}. The comparison between wetting free energies at different pore widths shows that the effect of the field grows with the thickness of the polarized water slab; however, the free energy change with the angle ϕ is essentially *independent* of the pore width. Given the smaller width amounts to about four layers of water molecules, it is clear that the angle dependence is dominated by pure surface-layer effects. The variation of the free energy with the angle produces an aligning torque of (absolute) magnitude

$$\tau(E, \phi) = -(\partial F/\partial \phi) \sim -A_{\mathrm{wl}} \partial \sigma(E, \phi)/\partial \phi \tag{17}$$

where F is the free energy and A_{wl} is the area of solid wall/liquid interface. The torque on nanopore walls arises solely due to anisotropic water/wall interactions and independently of any direct interaction between the wall material and the field. Importantly, because a major part of angular forces on water molecules reflects orientational preferences of hydrogen-bonding, a nonzero torque can exist even when there is no dielectric contrast between the pore material and water.

4.3.2 Dispersed Nanoparticles

The orienting effect, discussed above, is present in other geometries including nonspherical nanoparticles in a dispersion. As orientational forces between the solvent molecules and the particle surfaces couple with those imposed by the applied field, they augment the classical effect (16), and enhance the trend to align the nanoparticle surface with the field. This expectation, based on surface thermodynamics calculations for aqueous confinements [53], is confirmed in molecular dynamics simulations of freely rotating nano-platelets suspended in water under external field [108]. Orientational forces are found to *exceed* continuum theory predictions [129] by a factor close to two [108], providing a direct measure of the molecular mechanism neglected in macroscopic theories. Enhanced torques can considerably facilitate the use of electric field in tuning suspension structure and thus, for a supersaturated regime, also the structure of any emerging crystalline phase. For materials science as well as for the design of electro-mechanical sensors, it is essential to estimate also the *dynamics* of nanoparticle orientation. Reorientation time of a 2–3 nm wide graphene-like platelet under the (actual) field of ~0.03 V Å^{-1} is of O(10^2) ps. A very interesting result is an approximate balancing between increased hydrodynamic friction and the electric torque upon particle size scaling. The field-induced reorientation dynamics therefore depends only weakly on the particle size and remains fast O(10^2–10^3 ps) even for comparatively big O(10) nm particles; these results can be extrapolated to even bigger sizes not accessible by molecular dynamics simulations with explicit solvent. Apart from the torque enhancement due to hydration-shell molecules, the observed dynamic behavior conforms well to predictions [129] from classical hydrodynamics.

5 Conclusions

We have reviewed computational studies of neat water under combined effect of confinement and electric field. Molecular simulations in these systems were able to demonstrate remarkable differences between field-enhanced wetting *at the nanoscale* and in macroscopic systems. In particular, they highlighted the coupling between interfacial hydrogen bonds [100–103] and molecular alignment in the electric field. This coupling introduces a dependence of wetting on field direction and polarity in contrast to the conventional picture in macroscopic systems; system size plays a crucial role. The observed anisotropy in field-induced wetting is a new nanoscale phenomenon that has so far been elusive as, in the majority of current experimental setups, surface molecules represent a very low fraction of the total number of molecules affected by the field [130]. It may find applications, for example in the design of electrowetting techniques in fabrication and property tuning nanomaterials. Likewise, these effects may play a role in function of membrane proteins that are voltage sensitive, like pumps, transporters, and channels (Roux B, private communication, [131]), including artificial ones [132, 133].

Another novel mechanism that originates from molecular anisotropy of polar solvent molecules such as water reveals strong field-induced orientational forces acting on apolar surface through water mediation, which operate regardless of the presence or absence of solute/solvent permittivity difference. The findings have applications in nanomaterials engineering, where direct interactions between dipolar nanoparticles and applied electric field have been used to control and explain nanoassembly processes [134]. The new mechanism [53, 108] can be used in a similar way, regardless of the electrostatic nature of a nanoparticle. The water-mediated torques can act in concert with direct electrostatic interactions, and can be of similar magnitude when the particles are of nanosize. The response to the applied field takes place at an attractively short time scale [108]. Therefore, the mechanism can be considered in the development of chemical and biosensors.

The examples presented highlight the importance and predictive power of molecular modeling techniques in providing new insights into microscopic scale phenomena not fully accessible in experiment. The novelty of the results should have a broad impact in very active research fields of nano- and bioengineering, physics at the cell scale [135], etc. The future outlook calls for natural extensions of the work reviewed here: exciting new physics can emerge upon inclusion of aqueous salt solutions [136, 137] and evaluating the dynamic response of nanoconfined water to field change [138], a critical dynamic property for electro-switchable nanofluidic or optical devices.

Acknowledgements We thank Kevin Leung for his contribution to some of the work reviewed here. We gratefully acknowledge the financial support from the National Science Foundation (CHE-0718724) and the U.S. Department of Energy (DE-SC-0004406).

References

1. Berge B, Peseux J (2000) Variable focal lens controlled by an external voltage: an application of electrowetting. Eur Phys J E 3(2):159–163
2. Hendriks BHW, Kuiper S, Van As MAJ, Renders CA, Tukker TW (2005) Electrowetting-based variable-focus lens for miniature systems. Opt Rev 12(3):255–259
3. Stone HA, Stroock AD, Ajdari A (2004) Engineering flows in small devices: microfluidics toward a lab-on-a-chip. Annu Rev Fluid Mech 36:381–411
4. Squires TM, Quake SR (2005) Microfluidics: fluid physics at the nanoliter scale. Rev Mod Phys 77(3):977–1026
5. Cho SK, Moon H (2008) Electrowetting on dielectric (EWOD): new tool for bio/micro fluids handling. Biochip J 2(2):79–96
6. Dzubiella J, Allen RJ, Hansen JP (2004) Electric field-controlled water permeation coupled to ion transport through a nanopore. J Chem Phys 120(11):5001–5004
7. Dzubiella J, Hansen JP (2005) Electric-field-controlled water and ion permeation of a hydrophobic nanopore. J Chem Phys 122(23):234706
8. Rasaiah JC, Garde S, Hummer G (2008) Water in nonpolar confinement: from nanotubes to proteins and beyond. Annu Rev Phys Chem 59:713–740
9. Li JY, Gong XJ, Lu HJ, Li D, Fang HP, Zhou RH (2007) Electrostatic gating of a nanometer water channel. Proc Natl Acad Sci 104(10):3687–3692
10. Bostick D, Berkowitz ML (2003) The implementation of slab geometry for membrane-channel molecular dynamics simulations. Biophys J 85(1):97–107
11. Tieleman DP, Leontiadou H, Mark AE, Marrink SJ (2003) Simulation of pore formation in lipid bilayers by mechanical stress and electric fields. J Am Chem Soc 125(21):6382–6383
12. Tarek M (2005) Membrane electroporation: a molecular dynamics simulation. Biophys J 88(6):4045–4053
13. Suydam IT, Snow CD, Pande VS, Boxer SG (2006) Electric fields at the active site of an enzyme: direct comparison of experiment with theory. Science 313(5784):200–204
14. Bateni A, Susnar SS, Amirfazli A, Neumann AW (2004) Development of a new methodology to study drop shape and surface tension in electric fields. Langmuir 20(18):7589–7597
15. Bateni A, Laughton S, Tavana H, Susnar SS, Amirfazli A, Neumann AW (2005) Effect of electric fields on contact angle and surface tension of drops. J Colloid Interface Sci 283 (1):215–222
16. Shapiro B, Moon H, Garrell RL, Kim CJ (2003) Equilibrium behavior of sessile drops under surface tension, applied external fields, and material variations. J Appl Phys 93 (9):5794–5811
17. Quinn A, Sedev R, Ralston J (2003) Influence of the electrical double layer in electrowetting. J Phys Chem B 107(5):1163–1169
18. Daikhin LI, Kornyshev AA, Urbakh M (1999) The effect of electric field on capillary waves at the interface of two immiscible electrolytes. Chem Phys Lett 309(3–4):137–142
19. Holt JK, Park HG, Wang YM, Stadermann M, Artyukhin AB, Grigoropoulos CP, Noy A, Bakajin O (2006) Fast mass transport through sub-2-nanometer carbon nanotubes. Science 312(5776):1034–1037
20. Mugele F, Baret JC (2005) Electrowetting: from basics to applications. J Phys Condens Matter 17(28):R705–R774
21. Shamai R, Andelman D, Berge B, Hayes R (2008) Water, electricity, and between ... on electrowetting and its applications. Soft Matter 4(1):38–45
22. Mugele F (2009) Fundamental challenges in electrowetting: from equilibrium shapes to contact angle saturation and drop dynamics. Soft Matter 5(18):3377–3384
23. Mugele F, Duits M, van den Ende D (2009) Electrowetting: a versatile tool for drop manipulation, generation, and characterization. Adv Colloid Interface Sci 161(1–2):115–123
24. Bocquet L, Charlaix E (2010) Nanofluidics, from bulk to interfaces. Chem Soc Rev 39 (3):1073–1095

25. Guan L, Qi GC, Liu S, Zhang H, Zhang Z, Yang YL, Wang C (2009) Nanoscale electrowetting effects studied by atomic force microscopy. J Phys Chem C 113(2):661–665
26. Gelb LD, Gubbins KE, Radhakrishnan R, Sliwinska-Bartkowiak M (1999) Phase separation in confined systems. Rep Prog Phys 62(12):1573–1659
27. Luzar A, Bratko D, Blum L (1987) Monte-Carlo simulation of hydrophobic interaction. J Chem Phys 86(5):2955–2959
28. Lum K, Luzar A (1997) Pathway to surface-induced phase transition of a confined fluid. Phys Rev E 56(6):R6283–R6286
29. Nakanishi H, Fisher ME (1983) Critical-point shifts in films. J Chem Phys 78(6): 3279–3293
30. Evans R (1990) Fluids adsorbed in narrow pores – phase-equilibria and structure. J Phys Condens Matter 2(46):8989–9007
31. Schoen M, Diestler DJ (1998) Analytical treatment of a simple fluid adsorbed in a slit-pore. J Chem Phys 109(13):5596–5606
32. Klapp SHL, Schoen M (2002) Spontaneous orientational order in confined dipolar fluid films. J Chem Phys 117(17):8050–8062
33. Klapp SHL, Schoen M (2004) Ferroelectric states of a dipolar fluid confined to a slit-pore. J Mol Liq 109(2):55–61
34. Huang X, Margulis CJ, Berne BJ (2003) Dewetting-induced collapse of hydrophobic particles. Proc Natl Acad Sci 100(21):11953–11958
35. Parker JL, Claesson PM, Attard P (1994) Bubbles, cavities, and the long-ranged attraction between hydrophobic surfaces. J Phys Chem 98(34):8468–8480
36. Bratko D, Curtis RA, Blanch HW, Prausnitz JM (2001) Interaction between hydrophobic surfaces with metastable intervening liquid. J Chem Phys 115(8):3873–3877
37. MacDowell LG (2003) Formal study of nucleation as described by fluctuation theory. J Chem Phys 119(1):453–463
38. Israelachvili JN (2011) Intermolecular and surface forces, 3rd edn. Academic, London
39. Berne BJ, Weeks JD, Zhou RH (2009) Dewetting and hydrophobic interaction in physical and biological systems. Annu Rev Phys Chem 60:85–103
40. Evans R, Parry AO (1990) Liquids at interfaces – what can a theorist contribute. J Phys Condens Matter 2:SA15–SA32
41. Leung K, Luzar A, Bratko D (2003) Dynamics of capillary drying in water. Phys Rev Lett 90:065502
42. Koishi T, Yasuoka K, Ebisuzaki T, Yoo S, Zeng XC (2005) Large-scale molecular-dynamics simulation of nanoscale hydrophobic interaction and nanobubble formation. J Chem Phys 123(20):204707
43. Giovambattista N, Rossky PJ, Debenedetti PG (2006) Effect of pressure on the phase behavior and structure of water confined between nanoscale hydrophobic and hydrophilic plates. Phys Rev E 73(4):041604
44. Leung K, Luzar A (2000) Dynamics of capillary evaporation. II. Free energy barriers. J Chem Phys 113(14):5845–5852
45. Luzar A (2004) Activation barrier scaling for the spontaneous evaporation of confined water. J Phys Chem B 108(51):19859–19866
46. Luzar A, Leung K (2000) Dynamics of capillary evaporation. I. Effect of morphology of hydrophobic surfaces. J Chem Phys 113(14):5836–5844
47. Lum K, Chandler D (1998) Phase diagram and free energies of vapor films and tubes for a confined fluid. Int J Thermophys 19(3):845–855
48. Yushchenko VS, Yaminsky VV, Shchukin ED (1983) Interaction between particles in a nonwetting liquid. J Colloid Interface Sci 96(2):307–314
49. Yaminsky VV (2000) Molecular mechanisms of hydrophobic transitions. J Adhes Sci Technol 14(2):187–233
50. Giovambattista N, Lopez CF, Rossky PJ, Debenedetti PG (2008) Hydrophobicity of protein surfaces: separating geometry from chemistry. Proc Natl Acad Sci 105(7):2274–2279

51. Huang DM, Chandler D (2002) The hydrophobic effect and the influence of solute-solvent attractions. J Phys Chem B 106(8):2047–2053
52. Acharya H, Ranganathan S, Jamadagni SN, Garde S (2010) Mapping hydrophobicity at the nanoscale: applications to heterogeneous surfaces and proteins. Faraday Discuss 146:353
53. Bratko D, Daub CD, Luzar A (2009) Water-mediated ordering of nanoparticles in an electric field. Faraday Discuss 141:55–66
54. Sarupria S, Garde S (2009) Quantifying water density fluctuations and compressibility of hydration shells of hydrophobic solutes and proteins. Phys Rev Lett 103(3):037803
55. Lipmann G (1875) Relations entre les phenomenes electriques et capillaires. Ann Chim Phys 5:494
56. Buehrle J, Herminghaus S, Mugele F (2003) Interface profiles near three-phase contact lines in electric fields. Phys Rev Lett 91(8):086101
57. Vaitheeswaran S, Yin H, Rasaiah JC (2005) Water between plates in the presence of an electric field in an open system. J Phys Chem B 109(14):6629–6635
58. Frank HS (2023) J Chem Phys 1955:23
59. Mugele F, Klingner A, Buehrle J, Steinhauser D, Herminghaus S (2005) Electrowetting: a convenient way to switchable wettability patterns. J Phys Condens Matter 17(9):S559–S576
60. Krupenkin T, Taylor JA, Kolodner P, Hodes M (2005) Electrically tunable superhydrophobic nanostructured surfaces. Bell Labs Tech J 10(3):161–170
61. Vaitheeswaran S, Rasaiah JC, Hummer G (2004) Electric field and temperature effects on water in the narrow nonpolar pores of carbon nanotubes. J Chem Phys 121(16): 7955–7965
62. Dzubiella J, Hansen JP (2003) Reduction of the hydrophobic attraction between charged solutes in water. J Chem Phys 119(23):12049–12052
63. Dzubiella J, Hansen JP (2004) Competition of hydrophobic and Coulombic interactions between nanosized solutes. J Chem Phys 121(11):5514–5530
64. Brunet C, Malherbe JG, Amokrane S (2009) Controlling the composition of a confined fluid by an electric field. J Chem Phys 131(22):221103
65. Brunet C, Malherbe JG, Amokrane S (2010) Binary mixture adsorbed in a slit pore: field-induced population inversion near the bulk instability. Phys Rev E 82(2):021564
66. Bratko D, Daub CD, Leung K, Luzar A (2007) Effect of field direction on electrowetting in a nanopore. J Am Chem Soc 129(9):2504–2510
67. Maerzke KA, Siepmann JI (2010) Effects of an applied electric field on the vapor-liquid equilibria of water, methanol, and dimethyl ether. J Phys Chem B 114(12):4261–4270
68. Bratko D, Daub CD, Luzar A (2008) Field-exposed water in a nanopore: liquid or vapour? Phys Chem Chem Phys 10(45):6807–6813
69. England JL, Park S, Pande VS (2008) Theory for an order-driven disruption of the liquid state in water. J Chem Phys 128(4):044503
70. Landau LD, Lifshitz EM, Pitaevskii LP (1948) Electrodynamics of continuum media. Pergamon, Oxford
71. Høye JS, Stell G (1980) Statistical-mechanics of polar fluids in electric fields. J Chem Phys 72:1597
72. Frenkel D, Smit B (2002) Understanding molecular simulation, from algorithms to applications. Academic, San Diego
73. Allen MP, Tildesley DJ (1987) Computer simulation of liquids. Oxford University Press, New York
74. Frolich H (1990) Theory of dielectrics, 2nd edn. Oxford University Press, Oxford
75. Siepmann JI, Sprik M (1995) Influence of surface-topology and electrostatic potential on water electrode systems. J Chem Phys 102(1):511–524
76. Reed SK, Lanning OJ, Madden PA (2007) Electrochemical interface between an ionic liquid and a model metallic electrode. J Chem Phys 126(8):084704
77. Yeh IC, Berkowitz ML (1999) Ewald summation for systems with slab geometry. J Chem Phys 111(7):3155–3162

78. Yeh IC, Hummer G (2004) Diffusion and electrophoretic mobility of single-stranded RNA from molecular dynamics simulations. Biophys J 86(2):681–689
79. Sutmann G (1998) Structure formation and dynamics of water in strong external electric fields. J Electroanal Chem 450(2):289–302
80. Jia R, Hentschke R (2009) Dipolar particles in an external field: molecular dynamics simulation and mean field theory. Phys Rev E 80(5):051502
81. Berendsen HJC, Grigera JR, Straatsma TP (1987) The missing term in effective pair potentials. J Phys Chem 91(24):6269–6271
82. England JL, Pande VS (2010) Charge, hydrophobicity, and confined water: putting past simulations into a simple theoretical framework. Biochem Cell Biol 88(2):359–369
83. Wagner K, Keyes E, Kephart TW, Edwards G (1997) Analytical Debye-Huckel model for electrostatic potentials around dissolved DNA. Biophys J 73(1):21–30
84. Polk C (2000) Biological applications of large electric fields: some history and fundamentals. IEEE Trans Plasma Sci 28(1):6–14
85. Siu SWI, Bockmann RA (2007) Electric field effects on membranes: Gramicidin A as a test ground. J Struct Biol 157(3):545–556
86. Schweighofer KJ, Xia XF, Berkowitz ML (1996) Molecular dynamics study of water next to electrified Ag(111) surfaces. Langmuir 12(16):3747–3752
87. Kornyshev AA, Lee DJ, Leikin S, Wynveen A (2007) Structure and interactions of biological helices. Rev Mod Phys 79(3):943–996
88. Schweighofer KJ, Benjamin I (1995) Electric-field effects on the structure and dynamics at a liquid/liquid interface. J Electroanal Chem 391(1–2):1–10
89. Bratko D, Dolar D (1984) Ellipsoidal model of poly-electrolyte solutions. J Chem Phys 80 (11):5782–5789
90. Luzar A, Bratko D (1990) Electric double-layer interactions in reverse micellar systems – a Monte-Carlo simulation study. J Chem Phys 92(1):642–648
91. Bratko D, Woodward CE, Luzar A (1991) Charge fluctuation in reverse micelles. J Chem Phys 95(7):5318–5326
92. Wu JZ, Bratko D, Prausnitz JM (1998) Interaction between like-charged colloidal spheres in electrolyte solutions. Proc Natl Acad Sci 95(26):15169–15172
93. Wu JZ, Bratko D, Blanch HW, Prausnitz JM (1999) Monte Carlo simulation for the potential of mean force between ionic colloids in solutions of asymmetric salts. J Chem Phys 111(15):7084–7094
94. Svishchev IM, Kusalik PG (1994) Crystallization of liquid water in a molecular-dynamics simulation. Phys Rev Lett 73(7):975–978
95. Zangi R, Mark AE (2004) Electrofreezing of confined water. J Chem Phys 120(15): 7123–7130
96. Suresh SJ, Satish AV, Choudhary A (2006) Influence of electric field on the hydrogen bond network of water. J Chem Phys 124(7):074506
97. Suresh SJ (2007) Disruption of hydrogen bond structure of water near charged electrode surfaces. J Chem Phys 126(20):204705
98. Kiselev M, Heinzinger K (1996) Molecular dynamics simulation of a chloride ion in water under the influence of an external electric field. J Chem Phys 105(2):650–657
99. Rodgers JM, Weeks JD (2008) Local molecular field theory for the treatment of electrostatics. J Phys Condens Matter 20:494206
100. Luzar A, Svetina S, Zeks B (1983) The contribution of hydrogen-bonds to the surface-tension of water. Chem Phys Lett 96(4):485–490
101. Luzar A, Svetina S, Zeks B (1985) Consideration of the spontaneous polarization of water at the solid liquid interface. J Chem Phys 82(11):5146–5154
102. Lee CY, McCammon JA, Rossky PJ (1984) The structure of liquid water at an extended hydrophobic surface. J Chem Phys 80(9):4448–4455
103. Du Q, Freysz E, Shen YR (1994) Surface vibrational spectroscopic studies of hydrogen-bonding and hydrophobicity. Science 264(5160):826–828

104. Daub CD, Bratko D, Leung K, Luzar A (2007) Electrowetting at the nanoscale. J Phys Chem C 111(2):505–509
105. Grzelak EM, Errington JR (2010) Nanoscale limit to the applicability of Wenzel's equation. Langmuir 26(16):13297–13304
106. Grzelak EM, Errington JR (2008) Computation of interfacial properties via grand canonical transition matrix Monte Carlo simulation. J Chem Phys 128(1):014710
107. Hu GH, Xu AJ, Xu Z, Zhou ZW (2008) Dewetting of nanometer thin films under an electric field. Phys Fluids 20(10):102101
108. Daub CD, Bratko D, Ali T, Luzar A (2009) Microscopic dynamics of the orientation of a hydrated nanoparticle in an electric field. Phys Rev Lett 103:207801
109. Cramer T, Zerbetto F, Garcia R (2008) Molecular mechanism of water bridge buildup: field-induced formation of nanoscale menisci. Langmuir 24(12):6116–6120
110. Cheung DL (2010) Molecular simulation of nanoparticle diffusion at fluid interfaces. Chem Phys Lett 495(1–3):55–59
111. Eppenga R, Frenkel D (1984) Monte-Carlo study of the isotropic and nematic phases of infinitely thin hard platelets. Mol Phys 52(6):1303–1334
112. Bratko D, Jonsson B, Wennerstrom H (1986) Electrical double-layer interactions with image charges. Chem Phys Lett 128(5–6):449–454
113. Harismiadis VI, Vorholz J, Panagiotopoulos AZ (1996) Efficient pressure estimation in molecular simulations without evaluating the virial. J Chem Phys 105(18):8469–8470
114. Gloor GJ, Jackson G, Blas FJ, de Miguel E (2005) Test-area simulation method for the direct determination of the interfacial tension of systems with continuous or discontinuous potentials. J Chem Phys 123(13):134703
115. de Miguel E, Jackson G (2006) The nature of the calculation of the pressure in molecular simulations of continuous models from volume perturbations. J Chem Phys 125(16):164109
116. Brumby PE, Haslam AJ, de Miguel E, Jackson G (2011) Subtleties in the calculation of the pressure and pressure tensor of anisotropic particles from volume-perturbation methods and the apparent asymmetry of the compressive and expansive contributions. Mol Phys 109:169–189
117. Wang J, Bratko D, Luzar A (2011) Probing surface tension additivity on chemically heterogeneous surfaces: a molecular approach. Proc Natl Acad Sci USA 108(16):6374–6379
118. Leroy F, dos Santos D, Muller-Plathe F (2009) Interfacial excess free energies of solid-liquid interfaces by molecular dynamics simulation and thermodynamic integration. Macromol Rapid Commun 30(9–10):864–870
119. Bratko D (2010) General discussion. Fig. 2. Faraday Discuss 146:367–393
120. Giovambattista N, Debenedetti PG, Rossky PJ (2009) Enhanced surface hydrophobicity by coupling of surface polarity and topography. Proc Natl Acad Sci 106(36):15181–15185
121. Giovambattista N, Debenedetti PG, Rossky PJ (2007) Hydration behavior under confinement by nanoscale surfaces with patterned hydrophobicity and hydrophilicity. J Phys Chem C 111 (3):1323–1332
122. Zhang XY, Zhu YX, Granick S (2002) Hydrophobicity at a Janus interface. Science 295 (5555):663–666
123. Park J, Lu W (2007) Orientation of core-shell nanoparticles in an electric field. Appl Phys Lett 91(5):053113
124. Zhang X, Zhang ZL, Glotzer SC (2007) Simulation study of dipole-induced self-assembly of nanocubes. J Phys Chem C 111(11):4132–4137
125. Stratton JA (1941) Electromagnetic theory. McGraw-Hill, New York
126. Tsori Y (2009) Colloquium: phase transitions in polymers and liquids in electric fields. Rev Mod Phys 81(4):1471–1494
127. Froltsov VA, Klapp SHL (2007) Dielectric response of polar liquids in narrow slit pores. J Chem Phys 126(11):114703
128. Gramzow M, Klapp SHL (2007) Capillary condensation and orientational ordering of confined polar fluids. Phys Rev E 75(1):011605

129. Lyklema J (1991) Fundamentals in interface and colloid science, vol I: Fundamentals. Academic, London
130. Lu WY, Kim T, Han AJ, Chen X, Qiao Y (2009) Eletrowetting effect in a nanoporous silica. Langmuir 25(16):9463–9466
131. Anishkin A, Akitake B, Kamaraju K, Chiang CS, Sukharev S (2009) Hydration properties of mechanosensitive channel pores define the energetics of gating. J Phys Condens Matter 22(45):4120
132. Garate JA, English NJ, MacElroy JMD (2009) Carbon nanotube assisted water self-diffusion across lipid membranes in the absence and presence of electric fields. Mol Simul 35(1–2): 3–12
133. Garate JA, English NJ, MacElroy JMD (2009) Static and alternating electric field and distance-dependent effects on carbon nanotube-assisted water self-diffusion across lipid membranes. J Chem Phys 131(11):114508
134. Grzelczak M, Vermant J, Furst EM, Liz-Marzan LM (2010) Directed self-assembly of nanoparticles. ACS Nano 4(7):3591–3605
135. Sun S, Wong JTY, Zhang TY (2011) Molecular dynamics simulations of phase transition of lamellar lipid membrane in water under an electric field. Soft Matter 7(1):147–152
136. Girault HH (2006) Electrowetting: shake, rattle and roll. Nat Mater 5(11):851–852
137. Daub CD, Bratko D, Luzar A. Electric control of wetting by salty nanodrops: molecular dynamics simulations (submitted)
138. von Domaros M, Wang J, Bratko D, Kirchner B, Luzar A. Dynamics at a Janus interface (work in progress)